Materials Research Bulletin xxx (2008) xxx–xxx

Contents lists available at ScienceDirect

Materials Research Bulletin

journal homepage: www.elsevier.com/locate/matresbu

Nanostructured zinc oxide films synthesized by successive chemical solution deposition for gas sensor applications

O. Lupan [a,b,*], L. Chow [b], S. Shishiyanu [a], E. Monaico [c], T. Shishiyanu [a], V. Şontea [a], B. Roldan Cuenya [b], A. Naitabdi [b], S. Park [b], A. Schulte [b]

[a] Department of Microelectronics and Semiconductor Devices, Technical University of Moldova, 168 Stefan cel Mare Blvd., MD-2004 Chisinau, Republic of Moldova
[b] Department of Physics, University of Central Florida, 4000 Central Florida Blvd., Orlando, FL 32816-2385, USA
[c] National Center for Materials Study and Testing, Technical University of Moldova, 168 Stefan cel Mare Blvd., MD-2004 Chisinau, Republic of Moldova

ARTICLE INFO

Article history:
Received 16 June 2007
Received in revised form 1 April 2008
Accepted 4 April 2008
Available online xxx

Keywords:
A. Nanostructures
A. Oxides
B. Chemical synthesis
D. Electrical properties

ABSTRACT

Nanostructured ZnO thin films have been deposited using a successive chemical solution deposition method. The structural, morphological, electrical and sensing properties of the films were studied for different concentrations of Al-dopant and were analyzed as a function of rapid photothermal processing temperatures. The films were investigated by X-ray diffraction, scanning electron microscopy, energy dispersive X-ray spectroscopy, X-ray photoelectron and micro-Raman spectroscopy. Electrical and gas sensitivity measurements were conducted as well. The average grain size is 240 and 224 Å for undoped ZnO and Al-doped ZnO films, respectively. We demonstrate that rapid photothermal processing is an efficient method for improving the quality of nanostructured ZnO films. Nanostructured ZnO films doped with Al showed a higher sensitivity to carbon dioxide than undoped ZnO films. The correlations between material compositions, microstructures of the films and the properties of the gas sensors are discussed.

1. Introduction

Zinc oxide is a II–VI group semiconductor material with a direct bandgap of 3.37 eV (at 300 K), a large exciton binding energy (60 meV), and a Wurtzite structure similar to GaN [1]. ZnO has been investigated intensively due to its unique characteristics that may enable its efficient utilization in many commercial applications such as integrated optics, antireflection coatings, liquid crystal displays [1–5], piezoelectric [6,7], surface acoustic wave devices [1,8], electro- and photoluminescent devices [1], chemical and biological sensors [9,10]. More recently, zinc oxide has attracted considerable interest as a nanostructured material for thin film gas sensors in electronic noses [11,12], and as a nanostructured electrode material [13]. A major advantage of ZnO is that its properties can be readily modified and controlled by appropriate doping either by cationic (Al, In, Ga) or anionic (F) substitution [14], and by post-growth annealing. Investigations on nanostructured semiconducting oxide films for nanotechnology applications [15,16] demonstrated the potential to increase the gas response of ZnO films, since their performance is directly related to the exposed surface area, electrical and sensitivity characteristics.

Several techniques for synthesis from aqueous solution at low temperatures have been developed [17–27], and in particular the successive chemical solution deposition (SCSD) method [25]. It has proven to be a useful technique for growing nanostructured ZnO thin films [21,22,26]. The SCSD is a simple and flexible method which offers an easy way to dope film through a well-controlled heterogeneous reaction. It does not require high quality substrates with planar surfaces, and it can be operated at room temperature without the need for vacuum. Growth parameters are relatively easy to control, and stoichiometric deposition with different grain structures can be realized [25–27,9]. However, the SCSD synthesis of Al-doped ZnO (AZO) films and effect of post-grown rapid photothermal processing (RPP) of nanostructured doped ZnO has not been extensively studied.

In this paper we present results on SCSD synthesis as well as the effects of Al dopants and rapid photo thermal processing temperature on structure, morphology, Raman spectra and X-ray photoelectron spectroscopy (XPS) characteristics of nanostructured ZnO thin films. The combined results demonstrate the potential to improve the carbon dioxide gas sensor response of SCSD grown ZnO thin films.

* Corresponding author at: Department of Microelectronics and Semiconductor Devices, Technical University of Moldova, 168 Stefan cel Mare Boulvard, MD-2004, Chisinau, Republic of Moldova. Tel.: +373 22 509914; fax: +373 22 509910.
E-mail addresses: lupanoleg@yahoo.com, lupan@physics.ucf.edu (O. Lupan).

0025-5408/$ – see front matter © 2008 Elsevier Ltd. All rights reserved.
doi:10.1016/j.materresbull.2008.04.006

2. Experimental

2.1. Successive chemical solution deposition (SCSD)

Undoped, as well as Al-doped ZnO thin films have been deposited on Corning glass and Si substrates by the SCSD method. The glass substrates (35 mm × 50 mm × 0.05 mm) were cleaned in HCl (20%) solution for 10 min and then rinsed in deionized (DI) water (resistivity 18.2 MΩ cm). Subsequently the substrates were ultrasonically cleaned in ethanol:acetone (1:1) mixture for 5 min, rinsed again in deionized water and dried in a nitrogen gas flux. Then the substrates were sensitized according to [21]. After this protocol the glass substrates showed hydrophilic properties. A standard procedure described in Refs. [28,29] was used to clean the silicon substrate surfaces. Then the substrates were immersed vertically in the solutions for SCSD growth of ZnO thin films.

The aqueous zinc-ions solution complexed with NaOH was used as the cation precursor, in which reagents of zinc sulfate [$Zn(SO_4)\cdot 7H_2O$], aluminum sulfate [$Al_2(SO_4)_3\cdot 18H_2O$], and sodium hydroxide [NaOH] were used. The transparent complex solution was diluted with deionized water to obtain 0.05–0.15 M zinc concentration for deposition as described previously [21,23,29]. The pH value of the solution was about 10.5 in these experiments. The doping of ZnO films with Al was realized by adding the $Al_2(SO_4)_3\cdot 18H_2O$ in the aqueous solution corresponding to 0.5; 1; 2; 3 or 8% Al. The complex solution of cations and DI water for intermediate rinsing was kept at room temperature while the beaker with DI water as anionic precursor was kept at 95–98 °C during deposition.

The successive chemical solution deposition (SCSD) is based on the adsorption and reaction of the zinc complex ions from the aqueous complex solution, which is kept at room temperature. The immersion of the wet substrate in the anions solution kept at 95–98 °C during deposition. Between immersions, the substrate is rinsed with DI water at room temperature. In the SCSD of nanostructured ZnO thin films we followed four steps for a full growth cycle. As a first step the substrate was immersed in aqueous zinc-complex solution for 3 s in order to adsorb several layers of zinc complex ions on the substrate. The second step consisted of rinsing the sample in DI water for 2 s to remove loose zinc-complex ions to prevent homogeneous precipitation in the solution. In the third step, the substrate was reacted with anions from DI water as anionic precursor solution at 95–98 °C for 2 s and ZnO is formed on the interface. In the last step, the excess unreacted species and the reaction by-product were removed by dipping the substrate in DI water for 3 s. The deposition cycles were repeated until a desired thickness was obtained according to the previously studied growth kinetics [23,29]. Nanostructured ZnO thin films are produced with these procedures. The as-deposited ZnO nanostructured thin films (0.9 μm thickness) were dried in air at 150 °C for 5 min. However, by increasing the duration of the immersion procedure described above to 5 s in the first and third steps, and to >10 s in the second and fourth steps, one can realize a single ionic layer adsorption and reaction [20–21,30]. In this case we synthesized high-quality thin films with resistivity of less than $1 \times 10^{-3}\ \Omega$ cm, though they showed lower gas sensitivity compared to SCSD films. The details of tin- or nickel-doped zinc oxide films deposited by the successive single ionic layer adsorption and reaction (SILAR) method was reported elsewhere [21].

In order to investigate the effect of post-deposition annealing, films were rapid photo-thermal processed at temperatures between 300 and 750 °C in vacuum using an IFO-6 RPP system [28,29]. According to previous investigations, the optimum duration and temperature of post-growth RPP processing are 20 s and 650 °C, respectively [21,23,29]. The RPP processed pure ZnO and Al doped zinc oxide thin films samples are summarized in Table 1.

2.2. Characterization

The surface morphology of the nanostructured films was investigated with a VEGA TS 5130MM scanning electron microscope (SEM) equipped with Energy Dispersion X-ray Spectrometer (EDX). The film's thickness was measured using a Tencor P-10 profilometer and was confirmed by SEM cross-section measurements. For the cross-section measurements, the samples were cleaved and mounted in vertical position on an SEM holder. Several films were observed to assess the thickness measurements. The profilometer operating parameters included a scan length of 1000 μm and a scan speed of 20 μm/s. The composition of ZnO films was characterized by Rutherford Back Scattering (RBS) General IONEX 1.7 MV Tandetron and EDX. The ratio of Al and Zn in the doped film was investigated by the EDX measurements.

The phase structure of the deposited films was studied using Rigaku X-ray diffractometer (XRD) model 'D/B max' equipped with a high-intensity Cu Kα radiation (λ = 0.154178 nm) and optimized operating conditions of 30 mA and 40 kV at a scanning rate of 0.04°/s in the 2θ range of 10–90°.

An ultrahigh vacuum system (UHV) was used for electronic/chemical characterization. The analysis chamber is equipped with a hemispherical electron energy analyzer (Phoibos 100) and dual-anode (Al Kα, 1486.6 eV and Ag Lα, 2984.4 eV) monochromatic X-ray source (XR50, SPECS GmbH) for XPS. The base pressure in this chamber is $1–2 \times 10^{-10}$ mbar. Al Kα radiation was used in our studies.

Micro-Raman scattering experiments were performed with a Horiba Jobin Yvon LabRam IR system at a spatial resolution of 2 μm in a backscattering configuration. The 633 nm line of a He–Ne laser was used for off-resonance excitation with less than 4 mW of power at the sample. The spectral resolution was 2 cm^{-1}, and the instrument was calibrated to the same accuracy using a naphthalene standard.

The Al electrodes were deposited onto the surface of ZnO films in a vacuum system. The electrical characterization was performed using two-point probe method in the temperature range of 300–600 K. The *n*-type of conductivity exhibited by zinc oxide films was confirmed by using an Ecopia Hall effect measurement system.

To evaluate gas detection of the nanostructured ZnO films-based sensor a measuring apparatus was assembled. It consists of a closed quartz chamber connected to a gas flow system. The flow rate of test gases was measured using pre-calibrated mass flow meters. The mixed gas was flew through the chamber, in which the nanostructured ZnO films-based sensor was placed. A computer with suitable interface handled all controls and acquisition of data.

Table 1
The RPP processing of ZnO samples at 650 °C for 20 s

	ZnO pure	ZnO:Al (0.5%)	ZnO:Al(1%)	ZnO:Al (2%)	ZnO:Al (3%)	ZnO:Al (8%)
As-grown	0AZO	0.5AZO	1AZO	2AZO	3AZO	8AZO
After RPP	0AZOa	0.5AZOa	1AZOa	2AZOa	3AZOa	8AZOa

Please cite this article in press as: O. Lupan et al., Mater. Res. Bull. (2008), doi:10.1016/j.materresbull.2008.04.006

3. Results and discussions

3.1. Morphology characterization

The important growth parameters to tune SCSD film's morphology are the duration of substrate immersions in chemical solutions (from 30 to 1 s) and the number of successive dipping steps (from 4 to 1) in aqueous solution baths. Fig. 1 shows SEM images of the undoped and Al-doped ZnO films on glass substrate corresponding to samples (0AZO, 0.5AZO, 3AZOa and 8AZO) described in Table 1. For the estimation of mean nanoparticle size of nanostructured films, we drew a line on the SEM image and divided the length by the number of grain boundaries crossing the line. A mean particle dimension of 400 nm was calculated for the as-grown (sample 0AZO) and RPP ZnO films (sample 0AZOa). The independence of the surface morphology upon RPP till 650 °C was observed from SEM for pure and Al doped films. On the other hand, the morphology of films was found to be influenced by doping. For instance, Al doping in the concentration of 0.5–1.0% (samples 0.5AZO and 1AZO) reduces surface roughness and the mean nanoparticle dimension from 400 nm (sample 0AZO) to 100 nm (sample 0.5AZO) (see Fig. 1a and b) and allows one to obtain a more dense film, with higher surface-to-volume ratio. The morphology of samples 0.5AZO and 1AZO are similar. Doping with Al of ZnO films from 1% (sample 1AZO) to 3% (sample 3AZO) lead to increase of particle size from 100 to 200 nm following Fig. 1b and c, respectively. Doping with Al of ZnO films from 3% (sample 3AZO) to 8% (sample 8AZO) lead to increase of particle size (Fig. 1c and d), but also lead to the change of film structure. This behavior can be explained in terms of segregation of Al content into the grain boundaries. Once inside the grain boundary then become electrically inactive, which causes the increase in resistivity. Therefore, the samples with higher concentration (>3% Al) have not been studied further in our investigation.

3.2. Structural analysis

The XRD patterns of nanostructured ZnO films doped with 0.5% and 3% Al are shown in Fig. 2a and b, respectively. The influence of RPP on the XRD pattern is also studied and presented in Fig. 2a (curve 2) and b (curve 2). The diffraction peaks in the pattern can be indexed to hexagonal Wurtzite structured ZnO [space group: $P6_3mc$(186); a = 0.3249 nm, c = 0.5206 nm] and diffraction results are in agreement with JCPDS 036-1451 card for ZnO [31]. The intensity of the peaks relative to the background signal demonstrates high crystalline of the ZnO hexagonal phase of the products grown by SCSD. The characteristic peaks of $Zn(OH)_2$, Zn, Al, and Al_2O_3 were not observed. The nanocrystallites are oriented along the c-axis, direction with the highest intensity at the [0 0 2] direction. According to obtained results, it can be observed that doping of small amount of Al in the ZnO thin films promotes c-axis orientation. Moreover, for ZnO film doped above 3% Al, the c-axis orientation decreases according to our results shown in Fig. 2.

As one can see from Fig. 2, RPP leads to the increase of the intensity of (0 0 2) XRD peak by a factor of two in the investigated samples (0.5AZOa and 3AZOa—after RPP). This is indicative of a considerable improvement of the crystallinity as a result of RPP at 650 °C, 20 s. At the same time, the comparison of XRD patterns in Fig. 2a and b indicates on a considerable de-orientation of the crystal growth from the (0 0 2) direction with the increase of Al doping concentration from 0.5% to 3.0% (samples 0.5AZO and 3AZO, respectively).

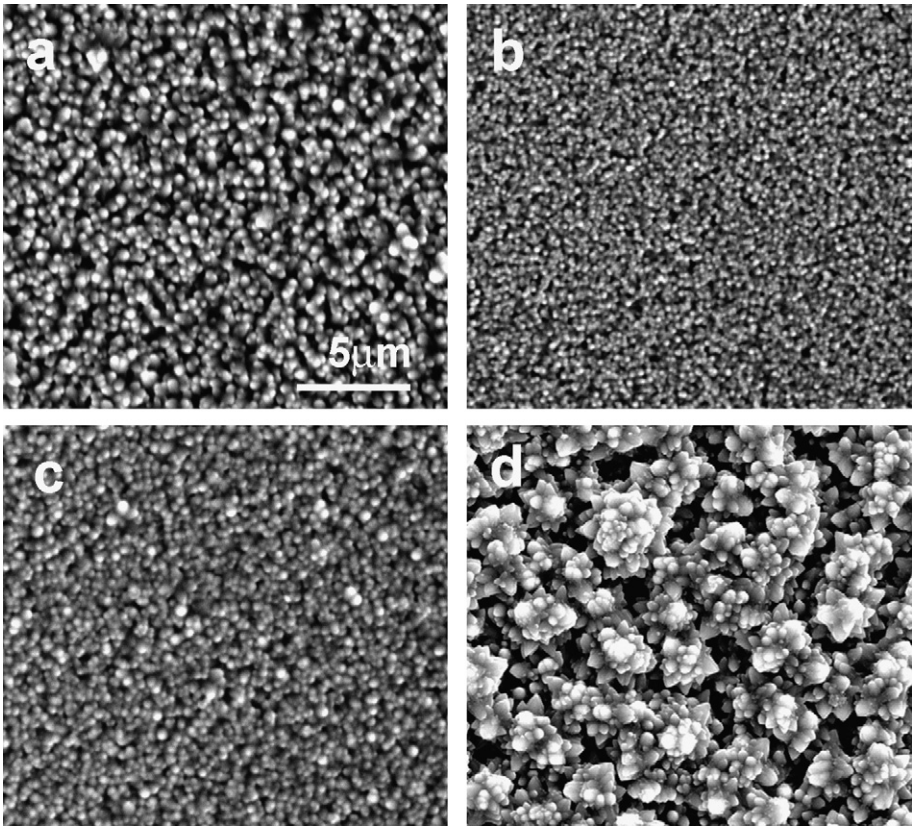

Fig. 1. Secondary electron micrographs of undoped and doped ZnO films onto glass substrates (corresponding to Table 1) showing the influence of doping and RPP annealing on surface morphology: (a) undoped as-grown film (sample 0AZO); (b) as-grown 0.5% Al-doped ZnO (sample 0.5AZO); (c) 3% Al-doped after RPP 650 °C, 20 s (sample 3AZOa); (d) as-grown 8% Al-doped (sample 8AZO). All images have the same magnification.

Please cite this article in press as: O. Lupan et al., Mater. Res. Bull. (2008), doi:10.1016/j.materresbull.2008.04.006

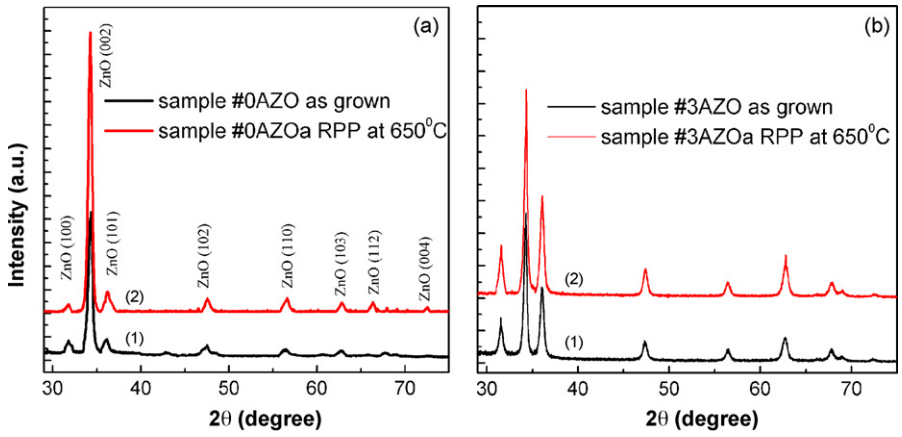

Fig. 2. The XRD pattern of the ZnO films with Al doping concentration of (a) 0.5% Al and (b) 3% Al; before (curve 1) and after RPP at 650 °C (curve 2), respectively.

The texture coefficient (T_C) for the (0 0 2) orientation is found to decrease from 3 to 2 with the increase of the Al concentration from 0.5% to 3.0% estimated from the following relation [32]:

$$T_C = \frac{I_{(002)}/I^0_{(002)}}{(1/N)\sum I_{(hkl)}/I^0_{(hkl)}} \quad (1)$$

where N is the number of diffraction peaks, $I_{(h\,k\,l)}$ and $I^0_{(hkl)}$ are the measured and corresponding recorded intensities according to the JCPDS (036-1451) card.

Another effect of Al doping in ZnO films is the shift of the (0 0 2) peak position to a low 2θ value with the increase of Al doping concentration. The position of this peak is shifted from 34.30° to 34.20° with the increase of Al concentration from 0.5% to 3.0%. This shift of the diffraction peak position indicates that films are in a uniform state of stress with tensile components parallel to *c*-axis [33,34]. The stress of the ZnO thin films was estimated employing the following formula [35,36]:

$$\sigma = -233 \times 10^9 \left(\frac{c_{film} - c_{bulk}}{c_{bulk}}\right) \text{Pa}, \quad (2)$$

where c_{bulk} is the strain-free lattice constant, and c_{film} is the lattice constant of the film.

According to XRD data, the stress value increases from -0.80×10^9 to -1.50×10^9 Pa with the increase of Al doping from 0.5 to 3.0 at.% (samples 0.5AZO and 3AZO, respectively). The RPP of the ZnO films with 3% Al concentration (samples 3AZO and 3AZOa) leads to the shift of the (0 0 2) peak position to 34.30°, which means that the stress is relaxed to the value -0.80×10^9 Pa.

The mean crystallite grain size (d) of the nanostructured ZnO samples, were calculated using Scherrer's formula [37]:

$$d = \frac{K\lambda}{(\beta^2 - \beta_0^2)^{1/2}} \cos\theta \quad (3)$$

where β is the measured broadening of a diffraction line peak, full width at half its maximum intensity (FWHM), β_0 is the instrumental broadening, $K = 180/\pi$, λ is the X-rays wavelength and θ is the Bragg diffraction angle. The average grain size determined from XRD line broadening is 240 and 224 Å for undoped ZnO (sample 0AZO) and Al-doped ZnO films (sample 0.5AZO), respectively. The crystal sizes were nearly the same for ZnO films before and after RPP, which is in agreement with previous results of Al-doped ZnO [38].

The Al/Zn ratios in films were analyzed by RBS and EDX measurement and were found a linear correlation in the investigated range 0–3%. The Al/Zn ratios surveyed are 1/99 and 3/97 (at.%) in different scanned regions on samples (1AZO) and (3AZO), respectively.

3.3. Chemical characterization (XPS) and Raman spectroscopy

X-ray photoelectron spectroscopy (XPS) was used to monitor changes in the stoichiometry and oxidation state of pure and Al-doped ZnO thin films. Fig. 3 shows XPS spectra from the C 1s (a), O

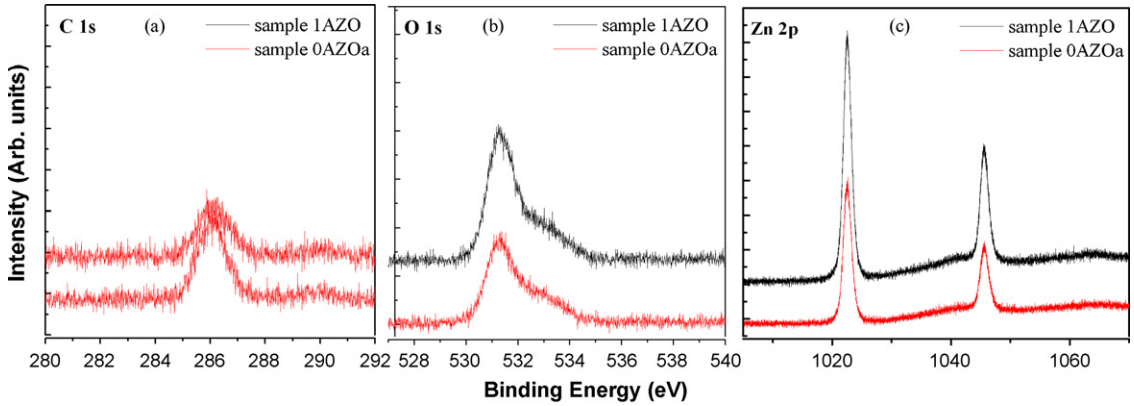

Fig. 3. XPS spectra (Al Kα = 1486.6 eV) corresponding to the (a) C 1s, (b) O 1s, and (c) Zn 2p core levels of ZnO films supported on glass and measured at room temperature. The ZnO films had the following dopants: none (sample 0AZOa) and Al-doped (sample 1AZO). The samples RPP annealed to 650 °C for 20 s prior to the XPS measurements are labeled as "a".

Please cite this article in press as: O. Lupan et al., Mater. Res. Bull. (2008), doi:10.1016/j.materresbull.2008.04.006

1s (b), and Zn 2p (c) core level regions of ZnO films measured after two different thermal treatments at 150 °C (sample 1AZO), and RPP at 650 °C (sample 0AZOa). Charging effects due to the low conductivity of the glass slides used as substrates have been minimized by calibrating the binding energy (BE) scale using the O 1s XPS peaks of ZnO (531.2 eV) [39].

All samples show XPS peaks at ~1022.5 and ~1045.8 eV (Fig. 3c), corresponding to the $2p_{3/2}$ and $2p_{1/2}$ core levels of Zn in ZnO [40]. No differences were observed in the Zn-2p core levels of the ZnO films upon annealing to 650 °C (sample 0AZOa).

All samples show a clear photoelectron peak at ~531.2 eV, Fig. 3b, corresponding to the O 1s core level in ZnO [39]. This BE can be attributed to O 1s in SiO_2 [41], to oxidic species located at the surface of ZnO films (shifted +1.8 eV with respect to O 1s in bulk-like ZnO) [42], as well as to hydroxide species [42]. Since the thickness of the ZnO films was 0.9 μm, no XPS signal from the SiO_2 substrate is expected. However, since this signal does not completely disappear after annealing at 650 °C, we can attribute the shoulder in our O 1s spectra to surface oxygen species on ZnO surface.

Representative Raman spectra (RS) of the nanostructured ZnO films are shown in Fig. 4. The dominant peaks are at 100 and 438 cm^{-1}, which are indicative of the Wurtzite structure ZnO [43], and are attributed to the low- and high-E_2 mode of non-polar optical phonons, respectively. Fig. 4 presents the Raman spectra of ZnO films doped with 0.5% (samples 0.5AZO and 0.5AZOa, curves 1 and 2) and 3% Al concentration (sample 3AZOa). The Raman spectra for 0.5% Al and 1.0% Al-doped ZnO are similar. The FWHM of the E_2(low) line is about 3 cm^{-1} which is another indication of the high quality of the SCSD synthesized nanocrystalline ZnO films. As one can realize from Fig. 4 (curve 2), RPP leads to the increase of the RS intensity suggesting the improvement of the film crystal quality, while the increase of Al doping to 3.0% concentration results in the decrease of the RS signal. This observation corroborates the XRD data.

3.4. Electrical properties

The pure ZnO films have a lower stability in corrosive, humid ambient due to large amount of oxygen (O) vacancy [44]. The properties of such zinc oxide films are often altered by adsorption of O_2 and water. Another factor limiting the application of pure ZnO as a transparent conductive film is its thermal instability. To overcome this disadvantages the properties of ZnO films are controlled by appropriate doping either by cationic (Al, In) or anionic (F) substitution [14] and post-growth annealing [21]. It has been documented [45] that the resistivity varies about 5% for temperature to increase from 50 to 400 °C in air when the content of Al in ZnO is 0.5–1.0%. The doping with Al in ZnO showed conductivity enhancement along with improved transparency [46,47] and mechanical stability [48]. Therefore, SCSD grown ZnO films have been doped with Al to improve their properties and electrical characteristics.

The electrical characterization was performed using two-point probe method and the *n*-type of conductivity and resistivity values exhibited by zinc oxide films was confirmed by Hall effect measurement.

Fig. 5 shows the electrical resistance of the undoped and Al doped ZnO thin films versus dopant concentration at room temperature and RPP annealing at 650 °C for 20 s. The electrical resistance decreases with Al doping as well as with rapid photothermal processing at 650 °C. The decrease of resistivity with Al-doping is due to the film crystallinity which results from smaller nanoparticles interconnected by local connections between them. The resistivity of AZO films is found to decrease with aluminum concentration up to 1.5 at.%. This can be explained by the fact that ionic radius of aluminum (Al^{3+} = 0.053 nm) is smaller than that of Zn (Zn^{2+} = 0.074 nm). So the resistivity decrease with the dopant concentration also is due to of the replacement of Zn^{2+}, by Al^{3+} ions and generation of a free charge carrier. But at concentrations of more than 3 at.% Al it will produce disorder in the lattice and increase scattering mechanism (proton and ionized impurity) which increase the resistivity [49,50]. Through the variation of the duration of maintenance in aqueous solutions during the four-step SCSD process, one can improve the crystallinity and tune the properties. The electrical resistance decreases with Al doping as well as with rapid photothermal processing at 650 °C. Note that this occurs simultaneously with the elimination of voids inside the pure and doped-ZnO films and increase surface-to-volume ratio, which is very important for gas sensor applications. Irreversible changes in the electrical characteristics have been observed when the ZnO films were subjected to post-growth rapid photothermal processing at temperatures higher than 300 °C for 20 s duration. In the temperature range of 550–650 °C, improvement of the crystallinity and stability of the ZnO sensor samples has been observed. The measurement has

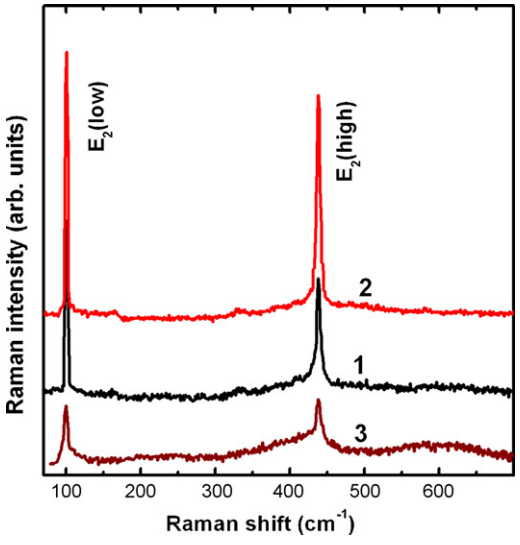

Fig. 4. Raman spectra of a ZnO film with the Al doping concentration of 0.5% before (curve 1) and after RPP at 650 °C (curve 2). Curve 3 is for a ZnO film with the Al doping concentration of 3.0% after RPP at 650 °C.

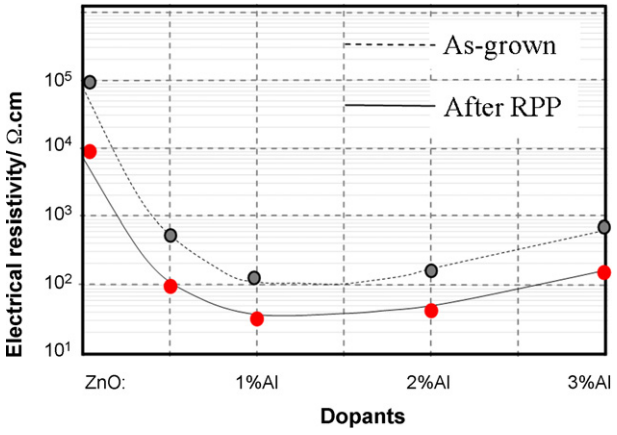

Fig. 5. Electrical resistivity values versus Al dopant concentration of the different ZnO films as-grown and after RPP at 650 °C for 20 s.

been carried out throughout 1 year period and it was determined that the Al-doped ZnO-based sensor elements have higher conductance stability, which ensures a stable zero level for gas sensor applications.

3.5. Gas sensing properties

Recently, carbon dioxide (CO_2) gas sensor have attracted considerably attention for applications in greenhouse gases (GHGs) monitoring. This type of sensors is also required for quality assurance of carbon dioxide used in soft drinks, mineral waters and beers according to The International Society of Beverage Technologists (ISBT) [51]. To assess the potential for such applications we investigated SCSD nanostructured ZnO films as sensing material for a novel carbon dioxide sensor.

For characterization of gas sensing properties, the sensor elements were placed in a 1000 cm^3 temperature controlled gas chamber. A typical gas measurements sequence consisted of predetermined intervals in which the sensor was exposed to gas atmospheres. After completion of one sequence the sensor and measurement cycle was repeated. The resistance response of each sensor structure was transformed into a sensitivity value using commonly used formula for the gases:

$$S = \left|\frac{R_{air} - R_{gas}}{R_{air}}\right|, \quad (4)$$

where R_{gas} is sensor resistance influenced by the carbon dioxide gas and R_{air} is the sensor resistance in the air. Fig. 6 shows the dynamic response of 1% Al-doped zinc oxide (sample 1AZOa) gas sensor to 1000 ppm carbon dioxide measured at room temperature. The gas sensitive ZnO:Al films treated at 650 °C exhibit the highest linear decrease of the resistivity with the gas concentration. The reaction time is about 20 s for sample with 1% Al-doped zinc oxide gas sensor at room temperature. The relative resistivity becomes stable after 20–25 s carbon dioxide exposure. The recovery time on the other hand, were restored to the 90% of the original level within 150 s suggesting a relatively longer recovery time, in comparison with the response time of ~20 s.

The adsorption–desorption sensing mechanism is proposed on the base of reversible chemisorption of the carbon dioxide on the nanostructured ZnO surface. It produces a reversible variation in the resistivity with the exchange of charges between carbon dioxide and the ZnO surface leading to changes in the depletion length [52]. Thus, one way to improve sensitivity is to increase the change in the surface/volume ratio [53]. It is well known that oxygen is adsorbed on a ZnO surface as O^- or O^{2-} by capturing electrons [54]. When Al-doped zinc oxide gas sensor is exposed to gas, the reversible chemisorption can take place:

$$CO_2 + V_O^{\bullet\bullet} + 2e' \leftrightarrow CO + O_O^x \quad (5)$$

where $V_O^{\bullet\bullet}$ is a double positive charged oxygen vacancies, e′ is negatively charged electron, O_O^x is neutral oxygen in oxygen site according to the Kröger–Vink notation [55].

This sensitivity was found to be useful for further development of carbon oxide sensors at room temperature for larger applications in GHGs monitoring and others.

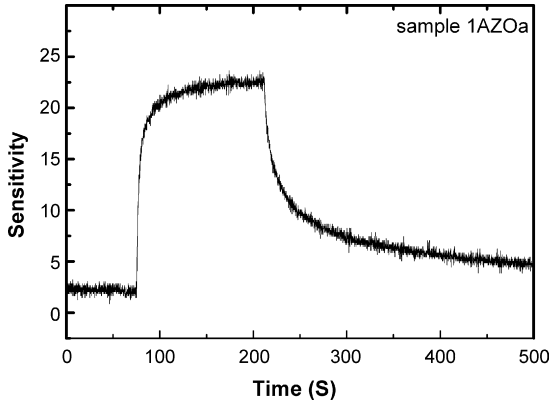

Fig. 6. The response time of a 1% Al-doped ZnO based sensor operated at room temperature towards Carbon dioxide gas.

4. Conclusion

Nanostructured ZnO and ZnO:Al thin films were synthesized by successive chemical solution deposition and rapid photothermal processing techniques. The advantages of this new technique derive from the simplicity of the process, short duration, energy save, accessible auxiliary materials, non-sophisticated equipment and structures with high efficiency. The morphological, electrical and sensing properties of zinc oxide films can be modified by controlling SCSD growth regimes, doping and post-growth RPP treatment conditions. The ZnO:Al films are nanocrystalline, but with a preferential orientation along the *c*-axis. The preferential orientation along (0 0 2) plane was enhanced with the RPP at 650 °C for 20 s and the thin films was uniform and nanostructure sized. The average grain size determined from XRD patterns is 240 and 224 Å for ZnO and Al-doped ZnO films, respectively. RPP improves the properties of ZnO:Al films, especially the crystallinity, electrical and sensing properties. The carbon dioxide sensitivity of Al-doped ZnO was improved by increasing surface-to-volume ratio of nanostructures.

These experimental results confirm that gas sensors based on aluminium-doped ZnO as sensitive layer are of great interest for gas detection. Moreover, successive chemical solution deposition allows the production of inexpensive nanocrystalline materials in a simple manner.

Acknowledgements

This work was made possible in part by an Award for young researchers (O.L.) No. "MTFP-1014B Follow-on" of the Moldovan Research and Development Association (MRDA) under funding from the U.S. Civilian Research & Development Foundation (CRDF). Financial support from the Ministry of Education and Science of Moldova (Project 321 b/s) and from Project 025P from the Supreme Council for Research and Technological Development of the Academy of Sciences of Moldova and the US National Science Foundation (DMR-0448491) are gratefully acknowledged. Raman measurements were supported by NSF MRI grant DMR-0421253.

References

[1] Ü. Özgür, Ya.I. Alivov, C. Liu, A. Teke, M.A. Reshchikov, S. Dogan, V. Avrutin, S.J. Cho, H.A. Morkoç, J. Appl. Phys. 98 (2005) 041301.
[2] K. Keis, E. Magnusson, H. Lindström, A. Holmberg, S.E. Lindquist, A. Hagfeldt, Sol. Energy Mater. Sol. Cells 73 (2002) 51.
[3] D. Mergerian, E. Malarkey, B. Newman, J. Lane, R. Weinert, B.R. McAvoy, C.S. Tsai, IEEE Ultrasonics Symp. (1978) 64.
[4] B.Y. Oh, M.C. Jeong, T.H. Moon, W. Lee, J.M. Myoung, J.Y. Hwang, D.S. Seo, J. Appl. Phys. 99 (2006) 124505.
[5] M. Chen, Z.L. Pei, C. Sun, J. Gong, R.F. Huang, L.S. Wen, Mater. Sci. Eng. B 85 (2001) 212.
[6] D. Jin, Z. Meng, J. Mater. Sci. Lett. 22 (2003) 971.
[7] T. Shiosaki, T. Yamamoto, A. Kawabata, R.S. Muller, R.M. White, Electron Device Meeting Int. 25 (1979) 151.
[8] H. Kim, Y. Lee, Y. Roh, J. Jung, M. Lee, H. Kwon, Ultrasonics Symp. IEEE Proc. 1 (1998) 323.
[9] H. Nanto, S. Tsubakino, T. Kawai, M. Ikeda, S. Kitagawa, M. Habara, J. Mater. Sci. 29 (1994) 6529.

[10] W.P. Tai, J.H. Oh, J. Mater. Sci.: Mater. Electron. 13 (2002) 391.
[11] H.K. Hong, C.H. Kwon, S.R. Kim, D.H. Yun, K. Lee, Y.K. Sung, Sens. Actuators B 66 (2000) 49.
[12] T. Hofmann, P. Schieberle, C. Krummel, A. Freiling, J. Bock, L. Heinert, D. Kohl, Sens. Actuators B 41 (1997) 81.
[13] K. Keis, S.E. Lindquist, A. Hagfeldt, in: Proceedings of the 13th Workshop on Quantum Solar Energy Conversion—(QUANTSOL 2001), Kirchberg in Tirol, Österreich, March 11–17, 2001.
[14] A.V. Singh, R.M. Mehra, A. Yoshida, A. Wakahara, J. Appl. Phys. 95 (2004) 3640.
[15] V.P. Tolstoy, Russ. Chem. Rev. 75 (2) (2006) 161.
[16] H. Rensmo, K. Keis, H. Lindstrom, S. Sodergren, A. Solbrand, A. Hagfeldt, S.E. Lindquist, L.N. Wang, M. Muhammed, J. Phys. Chem. B 101 (1997) 2598.
[17] M. Afzaal, P. O'Brien, J. Mater. Chem. 16 (2006) 1597.
[18] K. Govender, D.S. Boyle, P.B. Kenway, P. O'Brien, J. Mater. Chem. 14 (2004) 2575.
[19] P. Mitra, A.P. Chatterjee, H.S. Maiti, J. Mater. Sci.: Mater. Electron. 9 (1998) 441.
[20] S. Lindroos, M. Leskela, Int. J. Inorg. Mater. 2 (2000) 197–201.
[21] O.I. Lupan, S.T. Shishiyanu, L. Chow, T.S. Shishiyanu, Thin Solid Films 516 (10) (2008) 3338.
[22] T. Chou, J. Ting, Thin Solid Films 494 (2006) 291.
[23] S.T. Shishiyanu, T.S. Shishiyanu, O.I. Lupan, Sens. Actuators B 107 (2005) 379.
[24] A.E. Rakshani, Appl. Phys. A 81 (2005) 1497.
[25] A.E. Rakshani, J. Kokaj, J. Mathew, B. Peradeep, Appl. Phys. A 86 (2007) 377.
[26] M. Muhammed, Th. Tsakalakos, J. Kor. Ceram. Soc. 40 (11) (2003) 1027.
[27] Th.P. Niesen, M.R. De Guire, J. Electroceram. 6 (3) (2001) 169.
[28] S.T. Shishiyanu, O.I. Lupan, T.S. Shishiyanu, V.P. Şontea, S.K. Railean, Electrochim. Acta 49 (25) (2004) 4433.
[29] (a) S.T. Shishiyanu, O.I. Lupan, E. Monaico, V.V. Ursaki, T.S. Shishiyanu, I.M. Tiginyanu, Thin Solid Films 488 (2005) 15;
(b) O. Lupan, in: Proceedings of the 3rd International Conference on Microelectronics and Computer Science, vol. 1, Moldova, (2002), p. 149.
[30] S. Lindroos, M. Valkonen, M. Leskela, in: Proceedings of the Forum on New Materials of the 9th CIMTEC-World Ceramics Congress and Forum on New Materials Florence, Italy, June 14–19, (1998), p. 43.
[31] Joint Committee on Powder Diffraction Standards, Powder Diffraction File No. 036-1451.
[32] T. Mahalingam, K.M. Lee, K.H. Park, S. Lee, Y. Ahn, J.Y. Park, K.H. Koh, Nanotechnology 18 (2007) 035606.
[33] H. Deng, J.J. Russell, R.N. Lamb, B. Jiang, Thin Solid Films 458 (2004) 43.
[34] X.Z. Qiang, D. Hong, L. Yan, C. Hang, Mater. Sci. Semicond. Proc. 9 (2006) 132.
[35] Y.G. Wang, S.P. Lau, H.W. Lee, S.F. Yu, B.K. Tay, X.H. Zang, K.Y. Tse, H.H. Hng, J. Appl. Phys. 94 (2003) 1597.
[36] E. Senadin, H. Kavak, R. Esen, J. Phys.: Condens. Matter 18 (2006) 6391.
[37] (a) A.R. West, Solid State Chemistry, Wiley, New York, 1984, p. 174;
(b) T. Minami, H. Sato, K. Ohashi, T. Tomofuji, S. Takata, J. Cryst. Growth 117 (1992) 370.
[38] S.S. Lin, J.L. Huang, P. Sajgalik, Surf. Coat. Tech. 185 (2004) 254.
[39] C. Battistoni, J.L. Dormann, D. Fiorani, E. Paparazzo, S. Viticoli, Solid State Commun. 39 (1981) 581.
[40] S.W. Gaarenstroom, N. Winograd, J. Chem. Phys. 67 (1977) 3500.
[41] E. Paparazzo, J. Phys. D 20 (1987) 1091.
[42] F. Säuberlich, J. Fritsche, R. Hunger, A. Klein, Thin Solid Films 431/432 (2003) 378.
[43] Y.J. Xing, Z.H. Xi, Z.Q. Xue, X.D. Zhang, J.H. Song, R.M. Wang, J. Xu, Y. Song, S.L. Zhang, D.P. Yu, Appl. Phys. Lett. 83 (2003) 1689.
[44] D.J. Qiu, H.Z. Wu, A.M. Feng, Y.F. Lao, N.B. Chen, T.N. Xu, Appl. Surf. Sci. 222 (2004) 263.
[45] M. Chen, Z.L. Pei, C. Sun, J. Gong, R.F. Huang, L.S. Wen, Mater. Sci. Eng. B 85 (2001) 212–217.
[46] Z.L. Pei, C. Sun, M.H. Tan, J.Q. Xiao, D.H. Guan, R.F. Huang, L.S. Wen, J. Appl. Phys. 90 (2001) 3432.
[47] K. Postava, H. Sueki, M. Aoyama, T. Yamaguchi, K. Murakami, Y. Igasaki, Appl. Surf. Sci. 175/176 (2001) 543.
[48] S. Takata, T. Minami, H. Nanto, Thin Solid Films 135 (2) (1986) 183.
[49] B. Joseph, P.K. Manoj, V.K. Vaidyan, Ceram. Int. 32 (2006) 487.
[50] M. Mizuhashi, Thin Solid Films 76 (1981) 97.
[51] ISBT Carbon Dioxide Quality Guidelines and Analytical Procedure Bibliography, International Society of Beverage Technologists, USA, March 2001.
[52] H.L. Hartnagel, A.L. Dawar, A.K. Jain, C. Jagadish, Semiconducting Transparent Thin Films, IOP, Bristol, 1995.
[53] J. Riu, A. Maroto, F.X. Rius, Talanta 69 (2) (2006) 288.
[54] A.R. Raju, C.N.R. Rao, Sens. Actuators B 3 (4) (1991) 305.
[55] F.A. Kröger, in: R.N. Schock (Ed.), Point Defects in Minerals, American Geophysical Union, Washington, 1985, pp. 1–17.

Please cite this article in press as: O. Lupan et al., Mater. Res. Bull. (2008), doi:10.1016/j.materresbull.2008.04.006